Probabilistic Engineering Mechanics 73 (2023) 103481

Contents lists available at ScienceDirect

Probabilistic Engineering Mechanics

journal homepage: www.elsevier.com/locate/probengmech

A copula-based quantified airworthiness modelling for civil aircraft engines

Hang Zhou [a,b,*], Ajith Kumar Parlikad [b], Alexandra Brintrup [b], Andrew Harrison [c]

[a] James Watt School of Engineering, University of Glasgow, UK
[b] Institute for Manufacturing, Department of Engineering, University of Cambridge, UK
[c] Rolls-Royce plc, Derby, UK

ARTICLE INFO

Keywords:
Airworthiness
Aerospace engineering
Mechanical system reliability
Aviation industry
Statistical analysis

ABSTRACT

The aircraft engine serves as the core system of an aircraft and operates under extreme conditions, requiring high reliability and absolute safety. The design, manufacturing, and after-sales services of aircraft engines are complex processes. To ensure safety and performance, maintenance checks are performed periodically and hierarchically throughout the engine's life-cycle. Among these checks, shop visit (SV) heavy maintenance checks play a crucial role but are also costly, especially when they occur unexpectedly and unplanned. Analysis of the maintenance logbook, recording aviation operations, reveals a significant occurrence of unplanned SVs, which may be attributed to the existing maintenance policy based on a single time-definition. To address this issue, this paper seeks to establish a novel approach to quantifying airworthiness through copula modelling, which combines two time-definitions: the flying hour (FH) and the flying cycle (FC). This approach is unique in the aviation industry. By employing the Gumbel copula with the generalized extreme value (GEV) distribution as the marginal distribution, and utilizing non-parametric association measurement parameter estimation, the quantified airworthiness of civil aircraft engine fleets across multiple product lines can be effectively modeled. This research provides valuable insights into optimizing maintenance policies and enhancing the reliability and safety of aircraft engines.

1. Introduction

The study of reliability on complex engineering systems is fundamental to evaluating the general performance of system design. Highly reliable systems are particularly essential in key industries, including aerospace, infrastructure, energy, defense, etc. The study of reliability is not only valuable for maintaining the existing systems in peak performance but also in providing insights into the improvement of next-generation system design iterations.

Traditionally, the reliability study of engineering systems is the study of the probability that the system performs its designed purpose under stated conditions. The modelling of the system's reliability is the statistical analysis of both the system's available life and the system's consumed life, where the Weibull analysis is a classic probabilistic approach [1,2]. The available life of an engineering system is studied as a foundation for health monitoring across engineering disciplines, where the definition of life differs accordingly. For example, there are studies focused on natural time measurement including life in years for structural life estimation [3], in days for aircraft cooling systems [4], in hours and seconds for complex systems [5], as well as studies focusing on the count of cycles for system usages including studies on railway D-cables [6], and lithium-ion batteries [7]. However, when studying systems with multiple failure modes, the definition of life should not isolate the individual failure modes but should consider integrated life definitions enveloping all failure modes.

This is especially practical when statistically modelling the reliability of a system, such as the civil aircraft engine. The engine is highly complex in design, manufacturing, and maintenance, and it operates under extreme and critical conditions while demanding high reliability and absolute safety. Although failures may occur in any of the components within the sub-systems, it is crucial to ensure the consequences are understood and controlled. A typical civil aircraft engine consists of eight main sub-systems (modules): fan/low-pressure compressor (LPC), intermediate pressure compressor (IPC), high-pressure compressor (HPC), combustor (CBT), high-pressure turbine (HPT), intermediate pressure turbine (IPT), low-pressure turbine (LPT), and external gearbox [8], as shown in Fig. 1. The performance capability of the engine is determined by the combined performance of all modules and components. For a three-spool aircraft engine design, the combination of 'IPC+HPC+CBT+HPT+IPT' is referred to as the core sections or the hot sections. These sections endure the most critical conditions during aircraft operations. The engine's performance is monitored using exhaust gas temperature (EGT) during operations. The periodical shop visit (SV) involves heavy maintenance of the core sections and is based on the life limit parts (LLP) in those sections, which are measured

* Corresponding author at: James Watt School of Engineering, University of Glasgow, UK.
E-mail address: Hang.Zhou@glasgow.ac.uk (H. Zhou).

https://doi.org/10.1016/j.probengmech.2023.103481
Received 8 November 2022; Received in revised form 13 June 2023; Accepted 13 June 2023
Available online 21 June 2023

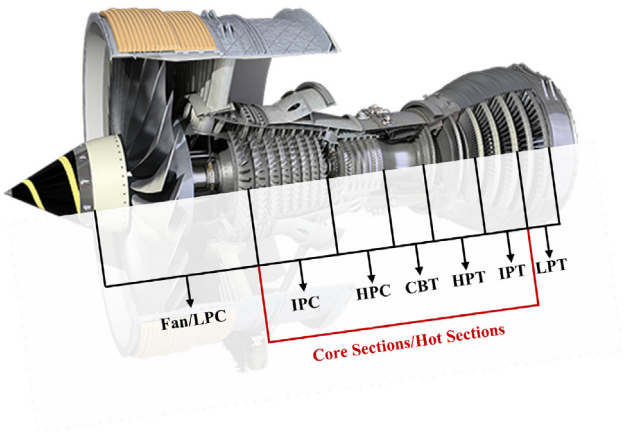

Fig. 1. Civil aircraft engine module overview.[1]

using flying cycles (FC). In addition to FC, the life of aircraft engines for business operations by airlines is also measured in flying hours (FH), primarily for performance restoration purposes to meet time-on-wing (TOW) targets. Each SV is highly costly, especially unplanned SVs. Analyzing real-life SV data reveals that the number of unplanned SVs exceeds expectations. This paper identifies the shortcomings of the current periodical maintenance check policy in the aviation industry, which is primarily based on the FC of the LLPs. It is proposed that maintenance checks should be planned based on the integrated reliability evaluations of both FH and FC. Considering that civil aircraft engines experience multiple deterioration mechanisms throughout their life-cycle, core components under cyclic loading suffer from fatigue-induced crack propagation. This phenomenon has been examined in studies on various diesel engines [9], and in the combustor sub-system of aircraft engines [10]. The cyclic loading-related failure mechanism determines the system's life in FC. Meanwhile, solid-material components in aircraft engines constantly work under extreme heat and are exposed to high-intensity stress, making creep an inevitable failure mechanism that controls the system's life in FH. Creep-related deterioration has been investigated in components like low-pressure turbine blade failures [11] and turbine disk failures, particularly in the widely used nickel-based superalloy material for such components [12]. The accumulation of dirt and dust on the tips of compressor and turbine blades also significantly influences the EGT, contributing to a loss of life in FH [8].

With reliability and safety being top priorities in aviation, this topic has attracted continuous studies and efforts for improvement from both academia and the industry. Modern aircraft are equipped with multiple sensors embedded into the systems to perform continuous health monitoring. To maximize monitoring effectiveness, methods such as the sensor performance metric are employed in aircraft fuel systems [13]. White and Karimoddini proposed the use of discrete event systems (DES) for detecting, isolating, and identifying fault occurrences during aircraft operations [14]. Health monitoring of aircraft is also important and valuable for fleet maintenance planning, and fleet simulations based on FCs of individual aircraft are conducted using agent-based modelling [15]. Much of the research on aircraft engine monitoring using sensor data focuses on the estimation of remaining useful life (RUL) [16,17]. These studies often utilize the popular C-MAPSS simulation dataset. However, these datasets simulate fewer than five failure modes, only consider failure modes related to FC, and do not fully reflect the complexity of real-life operations. Apart from the simulated datasets, there are also studies focusing on key components within the engine, such as aircraft engine bearings, based on FC usage [18]. Furthermore, one study focuses on predicting the long-term deterioration of a two-shaft commercial turbofan aircraft engine using real-life operational data. The study employs the Distance Based Sequential Aggregation with Gaussian Mixture Model (DBSA-GMM) approach, and the dataset includes 120 intact engine degradation cases with life consumption measured in FC [19]. Currently, only a few studies have been conducted on the long-term deterioration of aircraft engine reliability at the system level, even with a single time-definition.

A main reason for the shortfall in reliability studies in aviation and broader aerospace engineering is the significant lack of available real-life operational data, especially complete life-cycle maintenance data on large and comprehensive aircraft fleets. Recently, a few pioneering works in dual-time-definition reliability studies have emerged [20,21], providing valuable quantified data and modelling initiatives on single aircraft engine design products. This paper aims to extend these studies to further incorporate the complexity of mixed fleets by proposing dual-time-definition reliability modelling across multiple civil aircraft engine design product lines. This will enable the most comprehensive long-term reliability evaluation for engine fleets. In this study, the copula approach is considered due to its popularity in the combined evaluation of multiple variables. Its application in engineering studies has focused on identifying correlations among variables, including research on random motion errors in time-dependent motion and loading of a mechanism [22], analysis for multi-state parallel systems [23], especially with the consideration of cold standby [24], and estimation of slope failure probabilities based on correlations among slope height, slope angle, and shear strength parameters [25]. Regarding bivariate copula modelling performance, Tang et al. [26] further discussed the association of defined performance functions for reliability analysis when the marginal distribution and association parameters are known and fixed. However, none of the current copula studies consider the correlation of distinctive life definitions, limiting the current reliability modelling to a single dimension in time. Considering that this research extends the conventional reliability modelling to a higher dimension and that this high-dimensional modelling is unique to aviation systems, the proposed theories provide a comprehensive quantified airworthiness evaluation encompassing all potential failure modes. The quantified airworthiness modelling has the potential to redefine aviation operation strategies in both business and engineering operations.

This paper aims to propose novel approaches and make the following contributions:

(1) This research is based on the study of real-life operational data from three design models of civil aircraft engines with six different thrust ratings, which hold the highest market share. The study focuses on developing a quantified airworthiness model for these complex aviation systems, considering a variety of failure mechanisms in different modules and components that are the root causes for system removals and overhauls during SV heavy maintenance checks.
(2) Aircraft engines are designed to power aircraft, and although different design models share similarities in design and critical parts, they also differ in certain aspects. For example, engines designed for long-haul, medium-haul, and short-haul flights have different performance requirements. The engines can be categorized into system families, each containing several design sub-categories differentiated by thrust ratings. In this study, we consider that there should be statistical similarities in the quantified airworthiness for engine sub-categories within the same system family. These statistical similarities should be reflected in the marginal distributions of the quantified airworthiness model.
(3) The quantified airworthiness is fundamentally modeled using the copula approach. One challenge in developing a well-performed copula model lies in estimating the correlations between marginal distributions. Conventional parametric estimation of the association measurement parameter is not accurate when

[1]

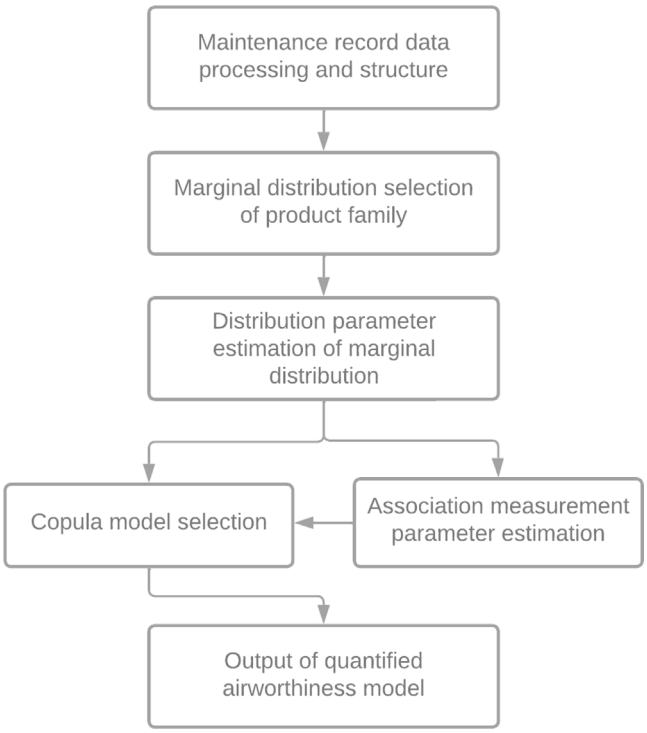

Fig. 2. Procedures of the quantified airworthiness modelling.

the marginal distributions do not exhibit obvious correlations. In this paper, we propose a non-parametric estimation of the association measurement parameter for copula modelling based on Monte Carlo simulation. This approach aims to improve the model accuracy and mitigate overfitting issues associated with such models.

This paper is structured as follows: In Section 2, the methodology of the main approaches and algorithms is presented and explained in detail. Section 3 provides the results and validation of the proposed methodology using modified real maintenance record data for fleets of aircraft engines. In Section 4, we further discuss the potential improvements of the proposed methodology and introduce our ongoing work, focusing on the development of the quantified airworthiness model as the foundation for building blocks.

2. Methodology

The determination of an applicable quantified airworthiness model requires several steps of optimization, particularly when the industry categorizes the system line into system families at a high level and each system family is further divided into system models for market segments and performance variety demands. For the aircraft engines studied in this research, a general design of the system represents a system family, such as the Trent 800, the Trent 1000, and the Trent XWB systems from Rolls Royce. Within each system family, there are different models with varying thrust levels. For example, the Trent 1000-E has a take-off thrust of 62264 lbf, the Trent 1000-G has 72066 lbf, and the Trent 1000-R has 81028 lbf. While these models share most of the same system design, the differences in thrust variations result in distinct operational conditions, failure patterns, and system reliability estimations. Considering this background, a flowchart illustrating the procedures for the development of a quantified airworthiness model is presented in Fig. 2.

2.1. Data processing & structure

Civil aircraft engines, as a specific type of complex aviation system, typically undergo thorough maintenance during shop visits before entering regular operations, thereby fully restoring their operational lifespan. The typical maintenance logbook records include the engines' operational history prior to maintenance, measured in dual-time-definitions of flying hours (FH) and flying cycles (FC). All maintenance activities are performed as a result of detecting and identifying at least one failure, categorized at a severity level requiring heavy maintenance checks. System i has a run-to-failure time record of (t_{1i}, t_{2i}), where t_{1i} (time-definition 1 in FH) and t_{2i} (time-definition 2 in FC) represent the system's safe operational life before failure. The maintenance record comprises a population of n systems.

2.1.1. Data normalization

Both time-definition 1 and time-definition 2 measurements are rational numbers. To ensure equal weighting for both measurements in estimating the system's life, a normalization step is performed. For the time-definition 1 measurement with the set $\mathbf{T_1} = (t_{11}, t_{12}, \dots, t_{1n})$ and the time-definition 2 measurements with the set $\mathbf{T_2} = (t_{21}, t_{22}, \dots, t_{2n})$, the upper boundary of time-definition 1 is determined by finding the largest sample within the set, denoted as $t_{1_{\text{upper}}} = \max\{t_{11}, t_{12}, \dots, t_{1n}\}$. Similarly, the upper boundary of time-definition 2 is obtained by identifying the largest sample within its set, given by $t_{2_{\text{upper}}} = \max\{t_{21}, t_{22}, \dots, t_{2n}\}$. These upper boundaries represent the maximum potential system life according to the system model. The lower boundaries for both time-definitions are set to 0. After normalization, both sets are as follows:

$$\begin{cases} \mathbf{T_{1_{norm}}} = \left(\frac{t_{11}}{t_{1_{\text{upper}}}}, \frac{t_{12}}{t_{1_{\text{upper}}}}, \dots, \frac{t_{1n}}{t_{1_{\text{upper}}}} \right) \\ \mathbf{T_{2_{norm}}} = \left(\frac{t_{21}}{t_{2_{\text{upper}}}}, \frac{t_{22}}{t_{2_{\text{upper}}}}, \dots, \frac{t_{2n}}{t_{2_{\text{upper}}}} \right) \end{cases} \tag{1}$$

2.1.2. Survival analysis

To conduct survival analysis on a population of bivariate normalized useful life records, the system capability is defined under bivariate coordinates as a vector composed of the normalized life by time-definition 1 and normalized life by time-definition 2. This vector is represented as $\overrightarrow{\mathbf{C_i}} = (\mathbf{T_{1_{norm}}}_i, \mathbf{T_{2_{norm}}}_i), i = 1, 2, \dots, n$. The magnitude of the vector is defined as follows:

$$C_i = \|\overrightarrow{\mathbf{C_i}}\| = \sqrt{\left(\frac{t_{1i}}{t_{1_{\text{upper}}}} \right)^2 + \left(\frac{t_{2i}}{t_{2_{\text{upper}}}} \right)^2} \tag{2}$$

The calculated C_i values are then combined with their associated t_{1i} and t_{2i} values to create the set $\mathbf{C} = (\mathbf{T_{1_{norm}}}, \mathbf{T_{2_{norm}}}, \mathbf{c})$. This set $\mathbf{C}$ is rearranged based on the ranking of C_i in $\mathbf{c}$, resulting in a monotonic increasing set of values. Let $\mathbf{C'} = (C_1', \dots, C_j', \dots, C_n')$ be the rearranged set, where $\mathbf{C'} = \mathbf{C}$ and $C_j \le C_{j+1}$. The two normalized time-definition measurements associated with capability C_j are denoted as $(\mathbf{T_{1_{norm}}}_j, \mathbf{T_{2_{norm}}}_j)$. A survival analysis, employing the Kaplan–Meier estimator [27], is then conducted based on the capability of each system in the population, as follows:

$$R(C_j') = \hat{S}(C_j') = \prod_{j: C_j' \le C_{\max}'} \left(1 - \frac{d_j}{n_j} \right) \tag{3}$$

In Eq. (3), d_j represents the number of systems recorded as failures at C_j', and n_j denotes the remaining number of systems in the population. The output of Eq. (3), $R(C_j')$, signifies the reliability of the system at C_j'. In the aviation industry, this reliability is often considered as a quantified measure of airworthiness, resulting in a three-dimensional description for each recorded data point with coordinates $(x, y, z) = (\mathbf{T_{1_{norm}}}_j, \mathbf{T_{2_{norm}}}_j, R(C_j'))$. This process generates a matrix for the dataset, where each row represents the normalized safe operational life in both FH and FC, along with the reliability at that specific time point. Column 1 represents the normalized time-definition 1 in FH for all data points, column 2 represents the normalized time-definition 2 in FC for all data points, and column 3 represents the reliability of all data points at

the respective time point. The values in column 3 are discrete and monotonically decreasing.

$$\mathbf{D} = \begin{pmatrix} \mathbf{T}_{\mathbf{1}_{\mathbf{norm}1}} & \mathbf{T}_{\mathbf{2}_{\mathbf{norm}1}} & R(C_1') \\ \mathbf{T}_{\mathbf{1}_{\mathbf{norm}2}} & \mathbf{T}_{\mathbf{2}_{\mathbf{norm}2}} & R(C_2') \\ \vdots & \vdots & \vdots \\ \mathbf{T}_{\mathbf{1}_{\mathbf{norm}j}} & \mathbf{T}_{\mathbf{2}_{\mathbf{norm}j}} & R(C_j') \\ \vdots & \vdots & \vdots \\ \mathbf{T}_{\mathbf{1}_{\mathbf{norm}n}} & \mathbf{T}_{\mathbf{2}_{\mathbf{norm}n}} & R(C_n') \end{pmatrix} \tag{4}$$

2.2. Selection of copula models

A copula is a function that joins or 'couples' a multivariate distribution function with its one-dimensional marginal distribution functions. Copulas have gained significant popularity in the field of high-dimensional statistical applications due to their ability to effectively model and estimate the distribution of random vectors by independently estimating the marginals and copulas. Numerous parametric copula families are available, typically characterized by parameters that govern the degree of dependence. According to Sklar's Theorem [28], let F be a bivariate joint distribution function of a continuous random variable X and Y with corresponding marginal distribution functions F_1 and F_2. There exists a copula $\mathscr{C}$ such that, for $-\infty < x_1 < \infty, -\infty < x_2 < \infty$, there is $F(x_1, x_2) = P(X_1 \le x_1, X_2 \le x_2) = \mathscr{C}(F_1(x_1), F_2(x_2))$. Sklar's theorem provides a foundation for combining marginal distributions into a joint copula function, which is particularly useful for Archimedean copula types [29]. This paper focuses on the four most commonly used copula models: the Gumbel copula, the Clayton copula, the Independence copula, and the Frank copula. Brief descriptions of these copula formats are provided to remind readers of their characteristics.

Gumbel copula. For a bivariate distribution, the Gumbel copula [30] is expressed as:

$$F(x_1, x_2) = exp\left\{-\left[\left(-logF_1(x_1)\right)^{\phi} + \left(-logF_2(x_2)\right)^{\phi}\right]^{1/\phi}\right\} \tag{5}$$

The Gumbel copula is a type of copula that exhibits tail dependence in only one corner. It is worth noting that an important characteristic of bivariate copula models is the calculation of the association measurement parameter ϕ, which describes the association relationship between the bivariate variables. In the case of the Gumbel copula, $\phi \in [1, \infty)$.

Clayton copula. The bivariate Clayton copula [31] is with the format of:

$$F(x_1, x_2) = \left[F_1(x_1)^{-\phi} + F_2(x_2)^{-\phi} - 1\right]^{-1/\phi} \tag{6}$$

For the Clayton copula, $\phi \in [-1, \infty)$ & $\phi \neq 0$.

Independence copula. When the association measurement parameter in the Gumbel copula $\phi = 1$, or when the parameter in the Clayton copula $\phi \to 0$. A special type of copula is created which is the independent copula [32]. With the format of:

$$F(x_1, x_2) = F_1(x_1)F_2(x_2) \tag{7}$$

It is obvious that the independence copula is free from the control of ϕ.

Frank copula. The fourth copula model being considered in this paper is the Frank copula [33], with the expression of:

$$F(x_1, x_2) = -\frac{1}{\phi} log\left[1 + \frac{\left(e^{-\phi F_1(x_1)} - 1\right)\left(e^{-\phi F_2(x_2)} - 1\right)}{e^{-\phi} - 1}\right] \tag{8}$$

For the Frank copula, $\phi \in [-1, 1]$ & $\phi \neq 0$.

It is evident that accurate estimation of the association measurement parameter ϕ is crucial for a reliable copula model. The calculation of the parameter ϕ for the four types of copula models is presented in Table 1.

Table 1
Relationship between association measurement parameter ϕ and Kendall's τ for four copula models.

Copula model	Kendall's τ
Gumbel	$\tau = \frac{\phi-1}{\phi}$
Clayton	$\tau = \frac{\phi}{\phi+2}$
Independence	NaN
Frank	$\tau = 1 - \frac{4}{\phi}\left(1 - \frac{1}{\phi}\int_0^{\phi} \frac{t}{e^t-1} dt\right)$

Table 2
Association measurement parameter ϕ calculation for four copula models.

Copula model	Association measurement parameter ϕ
Gumbel	$\phi = \frac{1}{1-\tau}$
Clayton	$\phi = \frac{2\tau}{1-\tau}$
Independence	NaN
Frank	Numerical solution

Two widely used methods for correlation analysis are Spearman's rank correlation coefficient [34] (Spearman's ρ) and Kendall's rank correlation coefficient [35] (Kendall's τ). In most cases, both rank correlation approaches are acceptable. However, this paper focuses on calculating the correlation using Kendall's τ approach. Kendall's τ is defined as follows:

$$\tau = \frac{n_c - n_d}{\sqrt{(n_0 - n_1)(n_0 - n_2)}} \tag{9}$$

where

$n_0 = \frac{n(n-1)}{2}$, $n_1 = \sum_i \frac{t_i(t_i-1)}{2}$, $n_2 = \sum_j \frac{u_j(u_j-1)}{2}$, n_c is the number of concordant pairs, n_d is the number of discordant pairs, t_i is the number of tied values in the ith group of ties for the first quantity, and u_j is the number of tied values in the jth group of ties for the second quantity.

The value of Kendall's τ is determined by the processed data from II. A is then substituted to the equations of τ in Table 1, and the values of the association measurement parameters are therefore obtained. The equations of the association measurement parameter upon obtaining Kendall's τ are shown in Table 2.

For the Frank copula, the association measurement parameter is typically calculated using numerical methods, as obtaining an analytical solution is challenging.

2.3. Parameter estimation

With the selection of the copula models introduced in II.B, the quantified airworthiness model is determined through four optimization steps, considering two key factors: the marginal distribution parameters and the copula model parameters. The parameter estimation for the marginal distribution involves two sub-categories: determining the choice of distribution and optimizing the parameters for the system family & system model. The estimation of the copula model also includes several sub-categories: parametric & non-parametric estimation of the association measurement parameter and the choice of copula model format. Fig. 3 illustrates these two factors with their respective sub-categories, and further detailed descriptions are provided.

2.3.1. Marginal distribution parameter estimation

The complexity of estimating marginal distribution parameters arises from the fact that a system type typically has a general design that is further developed into sub-design models. These sub-design models modify several components within the system to accommodate different usage purposes, as mentioned in the introduction. Therefore,

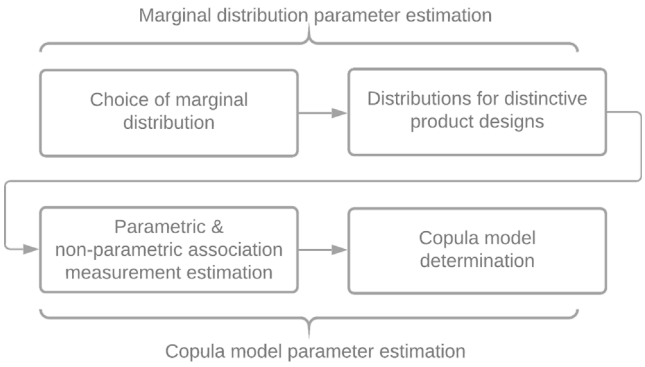

Fig. 3. Steps of copula model parameter estimation.

it is reasonable to assume that system models within the same system family share the same statistical distribution type [36,37]. This consideration is justified by design similarities and the need to avoid overfitting in statistical modelling for practicality. Let us consider a system design with M system families, where each system family is further divided into N_M system models. Each system model is denoted by PM_{IJ}, where $I \in [1, M], I \in \mathbb{Z}$, and $J \in [1, N_M], J \in \mathbb{Z}$. Each system model PM_{IJ} has a maintenance record for a population of O_{IJ} systems. By following the steps outlined in II.A, the normalized maintenance record considering bivariate measurements is represented as $\mathbf{D}_{IJ}$. To select the best marginal distribution for both time-definitions, the three most commonly used distribution formats in system reliability modelling are considered as potential candidates for all system families and models: the Weibull distribution (with shape and scale parameters), the Gumbel distribution (with location and scale parameters), and the generalized extreme value (GEV) distribution (with shape, location, and scale parameters). Each system model, on each time-definition, requires the estimation of either two or three parameters. However, computing the best choice of distribution based on the combined coefficient of determinations $\mathscr{R}^2$ for all system models becomes costly and infeasible when M and N_M are large. To overcome this challenge, this paper introduces a two-fold algorithm for estimating marginal distribution parameters.

Choice of marginal distribution. The targeted marginal distribution functions in the form of cumulative distribution functions (CDF) are listed below:

Marginal function as GEV distribution:

$$R(t) = 1 - e^{-\left[1+\xi\left(\frac{t-\mu}{\sigma}\right)\right]^{-1/\xi}} \tag{10}$$

Marginal function as Weibull distribution:

$$R(t) = e^{-(t/\sigma)^{\xi}} \tag{11}$$

Marginal function as Gumbel distribution:

$$R(t) = 1 - e^{-e^{-(t-\mu)/\sigma}} \tag{12}$$

The normal distribution is also included in this research as a benchmark for selecting the marginal distribution. Despite being less commonly used in the reliability evaluation of engineering systems, it is widely popular in statistics-related research. The cumulative distribution function (CDF) of the normal distribution can be expressed as:

$$R(t) = 1 - \frac{1}{2}\left[1 + \frac{2}{\sqrt{\pi}}\int_0^{\frac{t-\mu}{\sigma\sqrt{2}}} e^{-l^2} dl\right] \tag{13}$$

Eqs. (10) to (13) introduce the parameters used in this step. μ represents the location parameter, σ represents the scale parameter, and ξ represents the shape parameter. To perform this step, a representative system model is chosen from its corresponding system family. The selection of the representative model is based on the population size of maintenance records. For example, the representative model from family I contains the population of $O_{I_{\max}} = \max\{O_{I_1}, O_{I_2}, \ldots, O_{I_M}\}$. Creating the normalized dataset $\mathbf{D}_I = \{\mathbf{T}_{1_{\text{norm}I}}, \mathbf{T}_{2_{\text{norm}I}}, \mathbf{R}(C_I)\}, I = 1, 2, \ldots, M$. For this initial distribution model selection, all parameters for a candidate distribution are floated, meaning no value restriction is added to the fitting. The combined $\mathscr{R}^2$ for four potential reliability functions after fitting the most optimized sets of parameters $(\mu_{I_{\text{GEV}}}, \sigma_{I_{\text{GEV}}}, \xi_{I_{\text{GEV}}})$, $(\sigma_{I_{\text{Weibull}}}, \xi_{I_{\text{Weibull}}})$, $(\mu_{I_{\text{Gumbel}}}, \sigma_{I_{\text{Gumbel}}})$, and $(\mu_{I_{\text{Normal}}}, \sigma_{I_{\text{Normal}}})$. This calculation is performed on the records population of the representative model in family I at time-definition 1. The resulting $\mathscr{R}^2$ value is:

$$\sum_I \mathscr{R}_I{}^2 = \sum_{I=1}^{M}\left[1 - \frac{\sum_{Ii'=1}^{O_{I_{\max}}}(\mathbf{C}_{Ii'} - f_{Ii'})^2}{\sum_{Ii'=1}^{O_{I_{\max}}}(\mathbf{C}_{Ii'} - \frac{1}{O_{I_{\max}}}\sum_{Ii'=1}^{O_{I_{\max}}} C_{Ii'})}\right] \tag{14}$$

where

$$\begin{cases} f_{IGEV}(\mu,\sigma,\xi) = -e^{-\left[1+\xi_{IGEV}\left(\frac{T_{1norm_{Ii'}}-\mu_{IGEV}}{\sigma_{IGEV}}\right)\right]^{-1/\xi_{IGEV}}} \\ f_{IWeibull}(\sigma,\xi) = e^{-(T_{1norm_{Ii'}}/\sigma_{Weibull})^{\xi_{Weibull}}} \\ f_{IGumbel}(\mu,\xi) = 1 - e^{-e^{-(T_{1norm_{Ii'}}-\mu_{Gumbel})/\sigma_{Gumbel}}} \\ f_{INormal}(\mu,\sigma) = \frac{1}{2}\left[1 + \frac{2}{\sqrt{\pi}}\int_0^{\frac{T_{1norm_{Ii'}}-\mu_{Normal}}{\sigma_{Normal}\sqrt{2}}} e^{-l^2} dl\right] \end{cases} \tag{15}$$

The footnote i' in Eqs. (14) and (15) indicates that it applies to all data points within the processed dataset $\mathbf{D_I}$. By comparing the combined coefficient of determination $\mathscr{R}^2$ resulting from the fittings of all system models, the minimum value represents the best-fitting general distribution that describes one marginal distribution of the dataset. It is important to note that there is no explicit requirement for both marginal distributions to be of the same format.

Distribution for distinctive system designs. The second step in selecting the best fit is to estimate the parameters within each system model. To account for the fact that models within a system family share similar design structures and components, one parameter is fixed during the parameter optimization process for each individual system model (for distributions with two parameters) or two parameters are fixed (for distributions with three parameters). Previous studies on engineering systems have shown that fixing the scale parameter σ (for two-parameter distributions) or both the scale parameter σ and shape parameter ξ (for three-parameter distributions) is effective [36]. With this consideration, the location parameter μ becomes the key parameter for distinguishing multiple system models within a system family, while the scale parameter σ and shape parameter ξ become key parameters for distinguishing multiple system families. The fixed shape and scale parameters for the system family are obtained, and their values are denoted as σ_I and ξ_I for system family I. The location parameter for the distribution chosen for system model J_I in system family I is denoted as μ_{IJI}.

Let us take the GEV distribution as an example to illustrate the optimization of the location parameter for system family I with J_I system models. Consider the systems with properties shown in Table 3:

Further explanations on Table 3 are given here, in the column of 'Data Format', the data formats are generically written as, $(t_{I_M-1-O_{I_M}}, t_{I_M-2-O_{I_M}}, R_{I_M-O_{I_M}})$, the red color notation I_M represents the system model, the blue color notation 1 and 2 represent the two time-definition measurements, and the orange color notation O_{I_M} represent the label of data population in system model I_M records.

Table 3
Example dataset for marginal distribution parameter optimization.

System model (Family I)	Population	Data Format
Model I_1	O_{I_1}	$(t_{I_1-1-1}, t_{I_1-2-1}, R_{I_1-1})$, $(t_{I_1-1-2}, t_{I_1-2-2}, R_{I_1-2})$, …, $(t_{I_1-1-O_{I_1}}, t_{I_1-2-O_{I_1}}, R_{I_1-O_{I_1}})$
Model I_2	O_{I_2}	$(t_{I_2-1-1}, t_{I_2-2-1}, R_{I_2-1})$, $(t_{I_2-1-2}, t_{I_2-2-2}, R_{I_2-2})$, …, $(t_{I_2-1-O_{I_2}}, t_{I_2-2-O_{I_2}}, R_{I_2-O_{I_2}})$
…	…	…
Model I_{J_I}	$O_{I_{J_I}}$	$(t_{I_{J_I}-1-1}, t_{I_{J_I}-2-1}, R_{I_{J_I}-1})$, $(t_{I_{J_I}-1-2}, t_{I_{J_I}-2-2}, R_{I_{J_I}-2})$, …, $(t_{I_{J_I}-1-O_{I_{J_I}}}, t_{I_{J_I}-2-O_{I_{J_I}}}, R_{I_{J_I}-O_{I_{J_I}}})$
…	…	…
Model I_M	O_{I_M}	$(t_{I_M-1-1}, t_{I_M-2-1}, R_{I_M-1})$, $(t_{I_M-1-2}, t_{I_M-2-2}, R_{I_M-2})$, …, $(t_{I_M-1-O_{I_M}}, t_{I_M-2-O_{I_M}}, R_{I_M-O_{I_M}})$

The coefficient of determination for system Model I_{J_I} where $J_I = 1, 2, \ldots, M$ on time-definition 1 is:

$$\mathscr{R}_{I_{J_I}}{}^2 = 1 - \frac{SS_{res_{I_{J_I}}}}{SS_{tot_{I_{J_I}}}} = 1 - \frac{\sum_{\pi=1}^{O_{I_{J_I}}} \left\{ R_{I_{J_I}-\pi} - 1 - e^{-[1+\xi_I(\frac{t_{I_{J_I}-1-\pi}-\mu_{J_I}}{\sigma_I})]^{1-1/\xi_I}} \right\}}{\sum_{\pi=1}^{O_{I_{J_I}}} \left[R_{I_{J_I}-\pi} - \frac{1}{O_{I_{J_I}}} \sum_{\pi=1}^{O_{I_{J_I}}} (R_{I_{J_I}} - \pi) \right]^2} \tag{16}$$

In Eq. (16), π is used as the footnote notation for each data point within the dataset for system model I_{JI}. The objective is to obtain the optimized location parameter μ_{J_I} for each system model through the following equation:

$$\mathbf{M} = arg\max_{J_I} \left(\sum_M \mathscr{R}_{I_{J_I}}{}^2 \right) = arg\max_{J_I} \left(\sum_M \left\{ 1 - \frac{\sum_{\pi=1}^{O_{I_{J_I}}} \left\{ R_{I_{J_I}-\pi} - 1 - e^{-[1+\xi_I(\frac{t_{I_{J_I}-1-\pi}-\mu_{J_I}}{\sigma_I})]^{1-1/\xi_I}} \right\}}{\sum_{\pi=1}^{O_{I_{J_I}}} \left[R_{I_{J_I}-\pi} - \frac{1}{n_{I_{J_I}}} \sum_{\pi=1}^{O_{I_{J_I}}} (R_{I_{J_I}-\pi}) \right]^2} \right\} \right) \tag{17}$$

In Eq. (17), $\mathbf{M}$ represents the set that contains all the optimized location parameters μ_{J_I}. The solution to Eq. (17) is obtained by applying the multi-dimensional sparse grid search algorithm [38]. Using the demonstration of the GEV distribution example, it is possible to create the two marginal distributions for the two time-definitions as follows:

$$\begin{cases} F_{1IJ}(T_{1IJ} : \sigma_I, \xi_{IJI}, \mu_{IJI}) = Optimal\{R_{GEV}(T_{1IJ}), R_{Weibull}(T_{1IJ}), R_{Gumbel}(T_{1IJ})\} \\ F_{2IJ}(T_{2IJ} : \sigma_I, \xi_{IJI}, \mu_{IJI}) = Optimal\{R_{GEV}(T_{2IJ}), R_{Weibull}(T_{2IJ}), R_{Gumbel}(T_{2IJ})\} \end{cases} \tag{18}$$

Eq. (18) provides a description of the choice of the two marginal distributions, which are selected from the three potential distribution candidates. The choice of function and its parameters is based on the computation results of the most optimized coefficient of determination $\mathscr{R}^2$.

2.3.2. Copula model parameter estimation

The procedure following the selection of a marginal distribution for each variable is the construction of the bivariate copula model, which describes the joint distribution of the two marginal distributions. The choice of the copula model is based on two criteria: the format of the copula and the value of the association measurement parameter of the Archimedean copula.

Parametric & non-parametric association measurement parameter estimation. As introduced in Section 2.2, a direct method of calculating the association measurement parameter is through Kendall's τ. This parametric approach is used to combine the marginal distributions and form a bivariate distribution. However, in cases where the two variables defining the marginal distributions are distinct and do not exhibit obvious correlations, the parametric approach may not yield optimized results. In this section, a non-parametric approach to estimating the association measurement parameter is introduced as an alternative to the parametric approach. Considering that the copula is one approach to correlate the two marginal distributions, it is not assumed that all system reliability models require a uniform type of copula model in engineering applications. This leads to the estimation of the copula model and association measurement parameter on a case-by-case basis, depending on the system model. This paper proposes a Monte Carlo simulation-based algorithm for the non-parametric estimation of the association measurement parameter ϕ for copula models. The algorithm is presented as a two-step process, demonstrated in Algorithm 1 and Algorithm 2.

In Algorithm 1, $F(F_1, F_2)$ represents a copula model with determined marginal distributions F_1 and F_2. The proposed algorithms are applied to estimate the optimized ϕ for each of the four copula model candidates, using the given data.

Copula model determination. After obtaining the optimized ϕ value for the copula function, the sum of $\mathscr{R}^2$ values from the non-parametric approach is recalculated and compared with the $\mathscr{R}^2$ values directly calculated from the parametric approach. There are seven values to be compared, which are: Gumbel copula parametric result $\mathscr{R}^2_{Gumbel-_p}$, Gumbel copula non-parametric sum of errors $\mathscr{R}^2_{Gumbel-_n}$, Clayton copula parametric sum of errors $\mathscr{R}^2_{Clayton-_p}$, Clayton copula non-parametric sum or errors $\mathscr{R}^2_{Clayton-_n}$, Frank copula parametric sum of errors $\mathscr{R}^2_{Frank-_p}$, Frank copula non-parametric sum of errors $\mathscr{R}^2_{Frank-_n}$, and independence copula sum of errors $\mathscr{R}^2_{independence}$. The maximum $\mathscr{R}^2$ value determines both the choice of copula format and the association measurement parameter associated with the copula format.

2.4. Quantified airworthiness models

At the final step, with the choice of copula model F, the association measurement parameter ϕ_{opt}, the optimized marginal distribution F_1 for time-definition 1, and the optimized marginal distribution F_2 for time-definition 2, the quantified airworthiness model for the system model is given by:

$$R(T_1, T_2) = F(F_1, F_2 : \phi_{opt}) \tag{19}$$

To validate the versatility of the quantified airworthiness model, a statistical comparison is carried out across multiple system families with a variety of design models to assess the fitting accuracy.

3. Results & discussion

To demonstrate the practicality of the proposed algorithms, we applied the methodology to historical maintenance logbook records of three aircraft engine system families named Family 1, Family 2, and Family 3 in this study. Family 1 contains two datasets representing two system models, labeled Model 1 A and Model 1B. Similarly, Family 2 contains three system models: Model 2 A, Model 2B, and Model 2C. Family 3 consists of one system model labeled Model 3 A. A sample dataset provided in Table 4 indicates the format of the dataset, which

Algorithm 1 Monte Carlo Non-parametric ϕ estimation for copula

procedure ESTIMATION
  for $i \leftarrow 1, \upsilon$ **do**
    $\mathbf{D} \leftarrow (\mathbf{T_{1norm}}, \mathbf{T_{2norm}}, \mathbf{C})$ ▷ the processed dataset follows equation (4)
    $\mathbf{N} \leftarrow [1, 2, ..., n]$ ▷ Set of dataset labels with size n
    $\mathbf{N_{tr}} \leftarrow$ roundup$(p \times n)$ Integer(Random(1, n)) ▷ p is a percentage separating training set data label
    $\mathbf{N_{val}} \leftarrow \mathbf{N_{tr}}^{C}$ ▷ consider set **N** is Universe and set $\mathbf{N_{val}}$ is the Complement of set $\mathbf{N_{tr}}$
    $\mathbf{D_{tr}} \leftarrow \mathbf{D}[\mathbf{N_{tr}}]$ ▷ training dataset
    $\mathbf{D_{val}} \leftarrow \mathbf{D}[\mathbf{N_{val}}]$ ▷ validation dataset
    $\phi_{Optimize} \leftarrow arg\max_{i_{tr}} \left\{ 1 - \frac{\sum_{i_{tr}} \left\{ \mathbf{D_{tr}}[i_{tr},3] - F(F_1,F_2)|_{x=\mathbf{D_{tr}}[i_{tr},1],y=\mathbf{D_{tr}}[i_{tr},2]} \right\}^2}{\sum_{i_{tr}} \left\{ \mathbf{D_{tr}}[i_{tr},3] - \frac{\sum_{i_{tr}} \mathbf{D_{tr}}[i_{tr},3]}{roundup(p \times n)} \right\}^2} \right\}$ ▷ obtain optimized ϕ, by Algorithm 2
    $\mathbf{\Phi}[i] \leftarrow \phi$
    ${R_{val}}^2 \leftarrow \left\{ 1 - \frac{\sum_{i_{val}} \left\{ \mathbf{D_{val}}[i_{val},3] - F(M_1,M_2)|_{x=\mathbf{D_{val}}[i_{val},1],y=\mathbf{D_{val}}[i_{val},2]} \right\}^2}{\sum_{i_{val}} \left\{ \mathbf{D_{val}}[i_{val},3] - \frac{\sum_{i_{val}} \mathbf{D_{val}}[i_{val},3]}{n - roundup(p \times n)} \right\}^2} \right\}\Big|_{\phi}$ ▷ obtain R^2 for validation dataset by ϕ
    $\mathbf{R_{val}}[i] \leftarrow {R_{val}}^2$
  end for
  $\mathbf{U} \leftarrow [\mathbf{\Phi}, \mathbf{R_{val}}]$
  $\mathbf{U} \leftarrow$ sort $\mathbf{R_{val}}$ ▷ rank elements in **U** by R_{val} small to large
  $\mathbf{U'} \leftarrow \mathbf{U}[\upsilon - q, \upsilon]$ ▷ top q performance copula model
  $\phi \leftarrow \frac{\sum_{j=1}^{q} \mathbf{U'}[1,j]}{q}$
end procedure

Algorithm 2 Sub-algorithm for Algorithm 1 (Optimize ϕ in loop step)

procedure OPTIMIZE
  $\phi_1 \leftarrow \phi_{initial} \leftarrow \phi_{Parametric}$ ▷ set initial search value of ϕ
  for $l \leftarrow 2, \infty$ **do**
    for $u \leftarrow 0, 4$ **do**
      $\phi_l \leftarrow \phi_{l-1} + \frac{1}{10^u}$
      $R[l] \leftarrow \left\{ 1 - \frac{\sum_{i_{tr}} \left\{ \mathbf{D_{tr}}[i_{tr},3] - F(F_1,F_2)|_{x=\mathbf{D_{tr}}[i_{tr},1],y=\mathbf{D_{tr}}[i_{tr},2]} \right\}^2}{\sum_{i_{tr}} \left\{ \mathbf{D_{tr}}[i_{tr},3] - \frac{\sum_{i_{tr}} \mathbf{D_{tr}}[i_{tr},3]}{roundup(p \times n)} \right\}^2} \right\}\Big|_{\phi_l}$
      $l \leftarrow l + 1$
      $d \leftarrow R[l] - R[l-1]$
      $r \leftarrow \frac{R[l] - R[l-1]}{R[l-1]}$
      if $d \leq 0$ **then**
        $u = u + 1$
      else if $r \leq \rho$ **then** ▷ ρ is increment threshold
        BREAK
      end if
    end for
  end for
  $\phi_{Optimize} \leftarrow \phi_l$
end procedure

includes essential real-life operation data such as FH and FC for each run-to-failure record. Commonly the FH/FC ratio is to describe the flight profiles such as long-haul, medium-haul, or short-haul missions. The column 'Capability' indicates the run-to-failure time considering both time definitions.

The population of the logbook dataset for each distinctive engine design is as follows: Model 1 A with 327 entries, Model 1B with 101 entries, Model 2 A with 380 entries, Model 2B with 61 entries, Model 2C with 36 entries, and Model 3 A with 19 entries. By applying bivariate survival analysis on SV maintenance data to determine the quantified airworthiness for aviation operations, the deterioration of system reliability in relation to the operational life in terms of FH and FC is obtained. This information is presented in Fig. 4 as a scattered plot, where the example selected is system Family 1, Model 1B.

3.1. Marginal distribution format selection

The first key step towards developing the quantified airworthiness model is to determine the marginal distributions for all system families. Fig. 5 displays the best-fitted marginal distributions in four potential formats. In this figure, three representative system models, selected from three system families, are fitted with GEV, Gumbel, Weibull, and normal distributions on both time definitions. The navy-colored scatter plots represent the marginal distribution of reliability values for FH (system life on time-definition 1), while the green scatter plots represent the FC (time-definition 2). Table 5 presents the parameters of the fittings for the eight marginal distributions of the three representative models. As mentioned in the methodology section, all distribution formats share the same notation for parameters. In Table 5, σ represents

Table 4
Maintenance records after normalization.

System family	System model	Model number	Normalized FH	Normalized FC	Capability
1	1A	17	0.1331	0.1987	0.2392
...	...	...	...	...	...
1	1B	20	0.3442	0.2518	0.4265
...	...	...	...	...	...
2	2A	23	0.2440	0.4222	0.4876
...	...	...	...	...	...
2	2B	21	0.5571	0.5617	0.7911
...	...	...	...	...	...
2	2C	31	0.6914	0.6259	0.9326
...	...	...	...	...	...
3	3A	6	0.2235	0.2916	0.3674
...	...	...	...	...	...

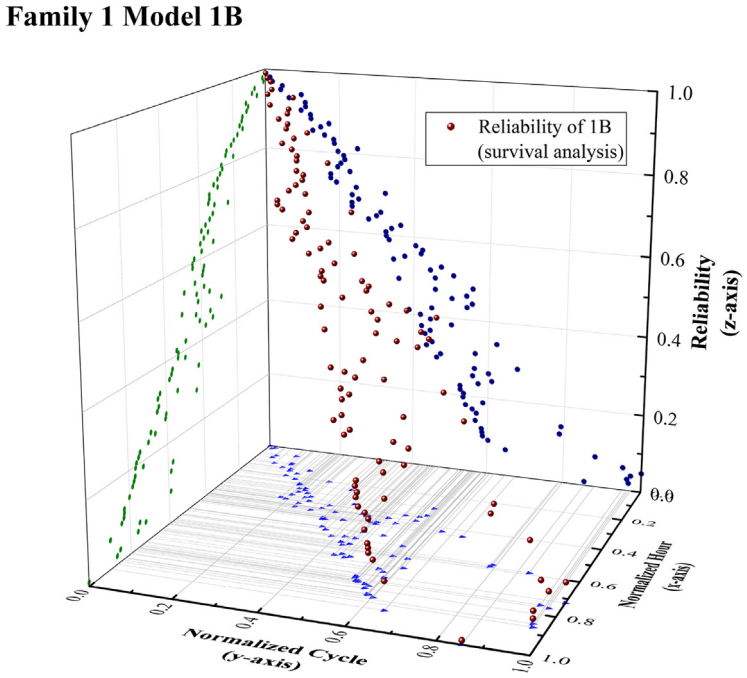

Fig. 4. Scattered airworthiness deterioration with survival analysis for system family 1 model 1B.

Table 5
Marginal distribution selection on two time-definitions for representative design models.

Distribution	Family 1 Model 1A		Family 2 Model 2A		Family 3 Model 3A	
	FH	FC	FH	FC	FH	FC
Weibull	$\sigma = 0.449$ $\xi = 1.756$	$\sigma = 0.434$ $\xi = 1.506$	$\sigma = 0.377$ $\xi = 1.394$	$\sigma = 0.299$ $\xi = 1.464$	$\sigma = 0.560$ $\xi = 1.047$	$\sigma = 0.656$ $\xi = 1.394$
Gumbel	$\sigma = 0.201$ $\mu = 0.289$	$\sigma = 0.216$ $\mu = 0.264$	$\sigma = 0.197$ $\mu = 0.222$	$\sigma = 0.149$ $\mu = 0.180$	$\sigma = 0.369$ $\mu = 0.294$	$\sigma = 0.359$ $\mu = 0.381$
Normal	$\sigma = 0.377$ $\mu = 0.232$	$\sigma = 0.360$ $\mu = 0.252$	$\sigma = 0.309$ $\mu = 0.232$	$\sigma = 0.242$ $\mu = 0.170$	$\sigma = 0.463$ $\mu = 0.426$	$\sigma = 0.539$ $\mu = 0.408$
GEV	$\sigma = 0.203$ $\mu = 0.290$ $\xi = -0.030$	$\sigma = 0.216$ $\mu = 0.264$ $\xi = -0.001$	$\sigma = 0.185$ $\mu = 0.217$ $\xi = 0.154$	$\sigma = 0.154$ $\mu = 0.182$ $\xi = -0.101$	$\sigma = 0.407$ $\mu = 0.318$ $\xi = -0.300$	$\sigma = 0.386$ $\mu = 0.395$ $\xi = -0.212$

the scale parameter, ξ represents the shape parameter, and μ represents the location parameter.

The evaluation of the marginal distribution is performed by calculating the sum of $\mathscr{R}^2$ values for the three representative models within each system family. This $\mathscr{R}^2$ based evaluation takes into account the sample size and balances the influence of both large and small sample populations. The results of the marginal distribution selection for the four potential distributions are presented in Table 6.

The evaluation domain for $\mathscr{R}^2$ is within the range of [0, 1]. A larger $\mathscr{R}^2$ value indicates a more accurate function fitting. Based on this criterion, the distribution format that yields the highest values of $\sum_I \mathscr{R}_I^2$ for all representative system models on both time-definitions is highlighted in red, while the second-highest values are highlighted in blue. Table 6 demonstrates that the GEV distribution produces the best-fitting results for both the FH time-definition marginal distribution and the FC time-definition marginal distribution. However, it should be noted that the

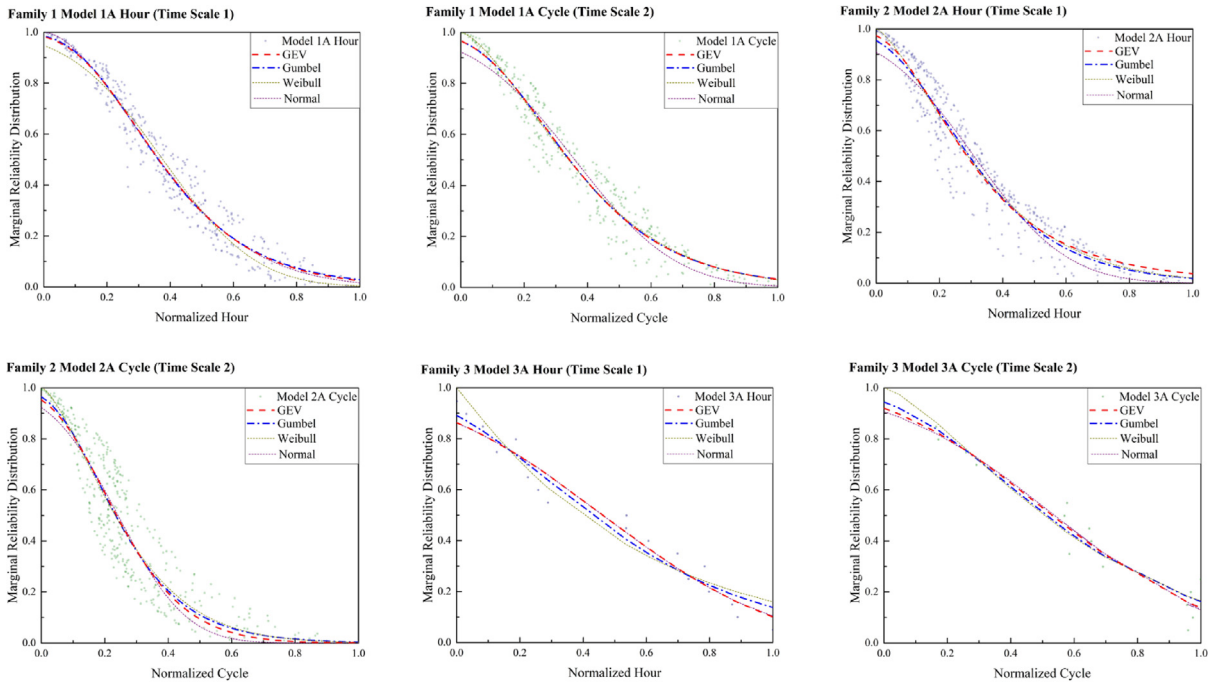

Fig. 5. Distribution fitting for each representative system model from three system families on both time definitions.

Table 6
Generic marginal distribution selection.

Distribution Format	FH ($\sum_I \mathscr{R}^2_{I_{FH}}$)	FC ($\sum_I \mathscr{R}^2_{I_{FC}}$)
Weibull	2.83389	2.75126
Gumbel	2.83950	2.75747
GEV	2.84412	2.75787
Normal	2.82176	2.73797

GEV distribution is a three-parameter distribution, unlike the Weibull, Gumbel, and normal distributions, which have fewer parameters. The presence of more parameters in a distribution increases the complexity of parameter optimization across multiple system families and models at a geometric growth rate. Comparing the GEV distribution to the Gumbel distribution, which has $\sum_I \mathscr{R}^2_I$ values highlighted in blue in Table 6, the Gumbel distribution is 0.16% smaller in FH measurement and 0.015% smaller in FC measurement. In this study, both the GEV and Gumbel distributions are carried forward to the next step due to their accuracy and performance as two-parameter distributions. It is important to note that the normal distribution exhibits the lowest accuracy in describing the marginal distribution, confirming that it is not a suitable choice for evaluating the airworthiness of the aircraft engine.

3.2. Marginal distribution parameter estimation

After identifying the GEV distribution and the Gumbel distribution as potential candidates for the marginal distributions of all system families, this step focuses on optimizing the distribution parameters by considering the similarity of each system model within the system families. As explained in the methodology, similar system models within a single system family share fixed distribution parameters. For the GEV distribution, the parameters that need to be determined are the scale parameter σ and the shape parameter ξ. In the case of the Gumbel distribution, only the scale parameter σ needs to be determined. In both distributions, the parameter that distinguishes different system models within a system family is the location parameter μ. To illustrate this process, let us consider system Family 1 with system Models 1 A and 1B in terms of FH. The optimization of the location parameter for the GEV distribution involves the following steps:

3.2.1. Step 1

Considering the fixed scale parameter $\sigma = 0.203$ and the fixed shape parameter $\xi = -0.030$ for both Family 1 Model 1 A and Family 1 Model 1B, the optimization of the location parameter μ is the sole variable to be optimized for each system model. The marginal FH for system 1 A and system 1B are denoted as t_{i_1} and t_{i_2}, respectively.

$$\mathscr{R}^2_{1A} = 1 - \frac{\sum_{i_1=1}^{327}\left\{R_{1_{i_1}} - 1 - e^{-[1-0.418(t_{i_1}-\mu_{1A})]^{1003/3}}\right\}}{\sum_{i_1=1}^{327}(R_{1_{i_1}} - \frac{1}{327}\sum_{i_1=1}^{327} R_{1_{i_1}})^2} \tag{20}$$

$$\mathscr{R}^2_{1B} = 1 - \frac{\sum_{i_2=1}^{101}\left\{R_{1_{i_2}} - 1 - e^{-[1-0.418(t_{i_2}-\mu_{1B})]^{1003/3}}\right\}}{\sum_{i_2=1}^{101}(R_{1_{i_2}} - \frac{1}{101}\sum_{i_2=1}^{101} R_{1_{i_2}})^2} \tag{21}$$

3.2.2. Step 2

The sum of $\mathscr{R}^2$ is considered and the target is to obtain the sum of μ_{1A} and μ_{1B} that maximizes $\sum_i \mathscr{R}^2$.

$$\begin{aligned}\mathbf{M}_{\mathbf{Family1-GEV}} &= [\mu_{1A}, \mu_{1B}] \\ &= arg\max_{1A,1B}\left(2 - \frac{\sum_{i_1=1}^{327}\left\{R_{1_{i_1}} - 1 - e^{-[1-0.418(t_{i_1}-\mu_{1A})]^{1003/3}}\right\}}{\sum_{i_1=1}^{327}(R_{1_{i_1}} - \frac{1}{327}\sum_{i_1=1}^{327} R_{1_{i_1}})^2}\right. \\ &\quad \left. - \frac{\sum_{i_2=1}^{101}\left\{R_{1_{i_2}} - 1 - e^{-[1-0.418(t_{i_2}-\mu_{1B})]^{1003/3}}\right\}}{\sum_{i_2=1}^{101}(R_{1_{i_2}} - \frac{1}{101}\sum_{i_2=1}^{101} R_{1_{i_2}})^2}\right)\end{aligned} \tag{22}$$

3.2.3. Step 3

Both candidate distributions, the GEV distribution and the Gumbel distribution, have had their location parameters optimized for each system model within the three system families. Consequently, the optimized distribution parameters for each system model in terms of both FH and FC, along with the combined R^2 for each design family, are presented in Table 7.

It can be observed from Table 7 that the GEV distribution exhibits a slight advantage in terms of $\mathscr{R}^2$, albeit marginal, with a difference

Table 7
Marginal distribution selection for the entire product line.

system Family & system Model	GEV Distribution		Gumbel Distribution	
	FH	FC	FH	FC
Family 1 Model 1A	$\sigma = 0.203$ $\mu = 0.290$ $\xi = -0.030$	$\sigma = 0.216$ $\mu = 0.287$ $\xi = -0.001$	$\sigma = 0.201$ $\mu = 0.289$	$\sigma = 0.216$ $\mu = 0.287$
Family 1 Model 1B	$\sigma = 0.203$ $\mu = 0.356$ $\xi = -0.030$	$\sigma = 0.216$ $\mu = 0.351$ $\xi = -0.001$	$\sigma = 0.201$ $\mu = 0.354$	$\sigma = 0.216$ $\mu = 0.351$
$\mathscr{R}^2$ Family 1	1.87140	1.87476	1.87133	1.87474
Family 2 Model 2A	$\sigma = 0.185$ $\mu = 0.217$ $\xi = 0.154$	$\sigma = 0.154$ $\mu = 0.220$ $\xi = -0.101$	$\sigma = 0.197$ $\mu = 0.222$	$\sigma = 0.149$ $\mu = 0.226$
Family 2 Model 2B	$\sigma = 0.185$ $\mu = 0.450$ $\xi = 0.154$	$\sigma = 0.154$ $\mu = 0.467$ $\xi = -0.101$	$\sigma = 0.197$ $\mu = 0.452$	$\sigma = 0.149$ $\mu = 0.464$
Family 2 Model 2C	$\sigma = 0.185$ $\mu = 0.266$ $\xi = 0.154$	$\sigma = 0.154$ $\mu = 0.299$ $\xi = -0.101$	$\sigma = 0.197$ $\mu = 0.271$	$\sigma = 0.149$ $\mu = 0.281$
$\mathscr{R}^2$ Family 2	2.74885	2.63326	2.73684	2.62225
Family 3 Model 3A	$\sigma = 0.417$ $\mu = 0.318$ $\xi = -0.3$	$\sigma = 0.386$ $\mu = 0.395$ $\xi = -0.212$	$\sigma = 0.369$ $\mu = 0.294$	$\sigma = 0.359$ $\mu = 0.381$
$\mathscr{R}^2$ Family 3	0.95766	0.95882	0.95483	0.95514

Table 8
Association measurement parameter ϕ and associated $\mathscr{R}^2$ evaluation for Family 1.

Copula Model	System	$\phi_{Parametric}$	$\mathscr{R}^2{}_{Parametric}$
Gumbel	Family 1 Model 1A	3.83	0.8981
	Family 1 Model 1B	3.33	0.9343
Clayton	Family 1 Model 1A	5.65	0.8919
	Family 1 Model 1B	4.67	0.9242
Frank	Family 1 Model 1A	13.43	0.8995
	Family 1 Model 1B	11.42	0.9307
Independence	Family 1 Model 1A	NaN	0.4950
	Family 1 Model 1B	NaN	0.6918

of less than 0.5%. These results indicate that for the studied aircraft engines, both the GEV and Gumbel distributions can be considered as options for marginal distributions, with a preference towards the GEV distribution.

3.3. Copula-based quantified airworthiness model

As discussed in the methodology section, the determination of the quantified airworthiness model relies on two stages: the formulation of the copula model and the estimation of the association measurement parameter. The estimation of the association measurement parameter is further divided into two approaches: the parametric approach and the non-parametric approach. The parametric approach is suitable for variables with simple and clear connections, while the non-parametric approach is considered a solution for variables with more complex connections. Both the parametric and non-parametric approaches are discussed in this research, with the parametric estimation serving as the baseline for the model's accuracy. Subsequently, the non-parametric approach is applied to compare against the baseline and determine the level of improvement.

3.3.1. ϕ Estimation for copula model — parametric approach

Family 1, consisting of Model 1 A and Model 1B, for example, contains 327 and 101 pairs of bivariate data points, respectively. The association measurement parameter ϕ for the four copula model candidates is listed in Table 8.

The obtained association measurement parameter determines the baseline quantified airworthiness model and is evaluated using $\mathscr{R}^2$, as listed in Table 9.

3.3.2. ϕ Estimation for copula model — non-parametric approach

Applying Algorithm 1 & 2 from the methodology, the purpose of the non-parametric approach is to improve the performance of the copula model through $\mathscr{R}^2$ evaluation. The iteration number v for the Monte Carlo simulation is set to 20, and the top-ranking performance model is selected as the top 20%, which gives a value of $q = 4$. The training dataset is set to be $p = 80\%$ of the entire dataset. The increment threshold at which the optimum search for ϕ stops is $\rho = 0.01\%$. It can be observed that for the estimation of the association measurement parameter ϕ using the parametric approach, the Frank copula best fits the dataset of Family 1 Model 1 A, while the Gumbel copula best fits Family 1 Model 1B. The non-parametric approach to estimating ϕ enhances the overall accuracy of the copula model fitting based on the determined marginal distributions. A comparison between the parametric and non-parametric approaches is presented in Table 10. The results support three observations: 1. The Gumbel copula performs well for both system models in Family 1 when using the non-parametric approach for ϕ estimation. 2. The non-parametric approach improves the copula modelling accuracy by 2.8% and 2.4% for Model 1 A, which has a data population of 327, and by 0.4% and 0.5% for Model 1B, which has a data population of 101. This indicates that as the dataset size for copula modelling increases, the association relationship

Table 9
Parametric and non-parametric approach comparison for system Family 1 data.

Copula Model	System	$\phi_{Parametric}$	$\mathscr{R}^2{}_{Parametric}$	$\phi_{non-Parametric}$	$\mathscr{R}^2{}_{non-Parametric}$	Improvement
Gumbel	Family 1 Model 1A	3.83	0.8981	17.49	0.9235	+2.8%
	Family 1 Model 1B	3.33	0.9343	5.28	0.9379	+0.4%
Frank	Family 1 Model 1A	13.43	0.8995	38.82	0.9214	+2.4%
	Family 1 Model 1B	11.42	0.9307	24.25	0.9358	+0.5%

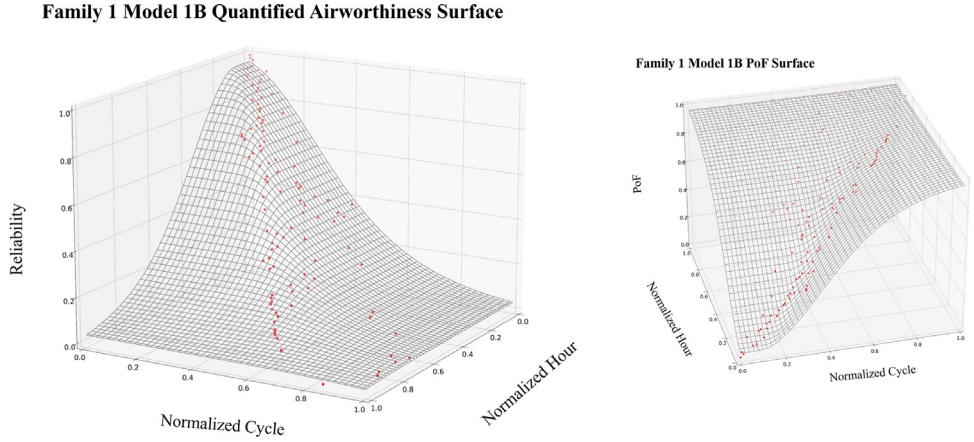

Fig. 6. Quantified airworthiness model and PoF for system Family 1 Model 1B.

Table 10
Validation of copula model performance on system Family 2 and Family 3.

System	Best copula model	$\mathscr{R}^2{}_{non-Parametric}$
Family 2 Model 2A	Gumbel	0.7178
Family 2 Model 2B	Gumbel	0.8621
Family 2 Model 2C	Clayton	0.8906
	Gumbel	0.8854
Family 3 Model 3A	Gumbel	0.9591

among marginal distributions becomes more complex. Hence, the non-parametric approach is more suitable for larger datasets, while the conventional parametric approach performs sufficiently well for smaller datasets. 3. Both copula models achieve high accuracy, with $\mathscr{R}^2 > 0.9$, demonstrating the effectiveness of using copulas to model the quantified airworthiness of civil aircraft engines.

To visualize the quantified airworthiness model, Fig. 6 presents the smooth copula surfaces based on the non-parametric ϕ estimation approach using the Gumbel copula. The figure demonstrates both the quantified airworthiness model and the probability of failure (PoF) surfaces.

The quantified airworthiness model for the civil aircraft engine Family 1 Model 1B is therefore given as:

$$F_{1B} = exp\left\{-\left[\left(-log\left(1-e^{-\left[1+-0.030\left(\frac{x-0.356}{0.203}\right)\right]^{-1/-0.030}}\right)^{5.28}\right.\right.$$
$$\left.\left.+\left(-log\left(1-e^{-\left[1+-0.001\left(\frac{y-0.351}{0.216}\right)\right]^{-1/-0.001}}\right)^{5.28}\right)\right]^{1/5.28}\right\} \quad (23)$$

3.4. Validation on all system families

To validate the applicability of the quantified airworthiness model, the methodology is further applied to two additional system families. The copula models, along with their corresponding model accuracy, are provided in Table 10.

The results provide evidence of the following: 1. The proposed algorithms generate $\mathscr{R}^2 > 0.7$ for all system families and model designs, irrespective of the data population. This demonstrates that the copula approach is highly accurate in modelling the quantified airworthiness of aircraft engines. 2. It is observed that the Gumbel copula is highly likely the best choice for modelling the life-cycle airworthiness of civil aircraft engines.

4. Conclusion & future work

This paper proposes a copula-based approach to evaluate the life-cycle reliability of civil aircraft engines by considering the joint operation lives of both FH and FC. This approach addresses the inadequacy of scheduling after-sales maintenance services for aviation systems when considering only FH or FC individually, which can lead to insufficient maintenance, and eventually turns into disastrous consequences. Due to the unique nature of the aviation industry, where the operation life is measured in two distinct time definitions, we define the copula-based bivariate reliability modelling for aviation systems as the quantified airworthiness model. This model has the potential to reshape the foundation for life-cycle operation planning in the aviation industry.

To validate the applicability of the quantified airworthiness model approach, six engine models from three distinctive propulsion system families were studied. The novel non-parametric estimation of the association measurement parameter for copula modelling achieved high accuracy across the entire product line. Additionally, it was discovered that the Gumbel copula, with GEV marginal distributions, is highly likely to serve as the generic quantified airworthiness model for the off-the-shelf civil aircraft engine product line.

However, despite the current accuracy of copula modelling, there is still room for improvement. One direction for improvement involves considering the tail dependence of the marginal distributions. The accuracy of the copula model in capturing tail correlations becomes crucial when evaluating situations with low airworthiness/high PoF. It is planned that future works will explore tail dependence. In addition to copula modelling, various applications built upon the quantified airworthiness model are being researched. These applications include a hierarchical maintenance work package recommender system, fleet

fast-response strategies, after-sales service pricing, and insurance & re-insurance for asset-heavy business models in the aviation industry.

Declaration of competing interest

The authors declare no conflict of interests.

Data availability

The data that has been used is confidential.

Acknowledgments

This research was funded by Aerospace Technology Institute, UK and Innovate UK through the TES-Digital (113174) project. The first author would like to express gratitude to the James Watt School of Engineering, University of Glasgow, UK, for providing ECR Funding and Start-up Funding to support the ongoing research. The first author would also like to thank the IMechE Airworthiness Committee for inspiring this research.

References

[1] T. Zhu, Reliability estimation for two-parameter Weibull distribution under block censoring, Reliab. Eng. Syst. Saf. (ISSN: 0951-8320) 203 (2020) 107071, http://dx.doi.org/10.1016/j.ress.2020.107071, URL https://www.sciencedirect.com/science/article/pii/S095183202030572X.

[2] H. Zhou, T.A.L. Genez, A. Brintrup, A.K. Parlikad, A hybrid-learning decomposition algorithm for competing risk identification within fleets of complex engineering systems, Reliab. Eng. Syst. Saf. (ISSN: 0951-8320) (2021) 107992, http://dx.doi.org/10.1016/j.ress.2021.107992, URL https://www.sciencedirect.com/science/article/pii/S0951832021005020.

[3] M.A. Vega, Z. Hu, T.B. Fillmore, M.D. Smith, M.D. Todd, A novel framework for integration of abstracted inspection data and structural health monitoring for damage prognosis of Miter gates, Reliab. Eng. Syst. Saf. (ISSN: 0951-8320) 211 (2021) 107561, http://dx.doi.org/10.1016/j.ress.2021.107561, URL https://www.sciencedirect.com/science/article/pii/S0951832021001149.

[4] I. de Pater, M. Mitici, Predictive maintenance for multi-component systems of repairables with remaining-useful-life prognostics and a limited stock of spare components, Reliab. Eng. Syst. Saf. (ISSN: 0951-8320) 214 (2021) 107761, http://dx.doi.org/10.1016/j.ress.2021.107761, URL https://www.sciencedirect.com/science/article/pii/S095183202100288X.

[5] Y. Cao, Y. Ding, M. Jia, R. Tian, A novel temporal convolutional network with residual self-attention mechanism for remaining useful life prediction of rolling bearings, Reliab. Eng. Syst. Saf. (ISSN: 0951-8320) (2021) 107813, http://dx.doi.org/10.1016/j.ress.2021.107813, URL https://www.sciencedirect.com/science/article/pii/S0951832021003355.

[6] Y. Zang, W. Shangguan, B. Cai, H. Wang, M.G. Pecht, Hybrid remaining useful life prediction method. a case study on railway D-cables, Reliab. Eng. Syst. Saf. (ISSN: 0951-8320) 213 (2021) 107746, http://dx.doi.org/10.1016/j.ress.2021.107746, URL https://www.sciencedirect.com/science/article/pii/S0951832021002775.

[7] F. Xu, F. Yang, Z. Fei, Z. Huang, K.-L. Tsui, Life prediction of lithium-ion batteries based on stacked denoising autoencoders, Reliab. Eng. Syst. Saf. (ISSN: 0951-8320) 208 (2021) 107396, http://dx.doi.org/10.1016/j.ress.2020.107396, URL https://www.sciencedirect.com/science/article/pii/S0951832020308838.

[8] S. Ackert, Engine maintenance concepts for financiers - elements of turbofan shop maintenance costs, 2011.

[9] L. Witek, M. Sikora, F. Stachowicz, T. Trzepiecinski, Stress and failure analysis of the crankshaft of diesel engine, Eng. Fail. Anal. (ISSN: 1350-6307) 82 (2017) 703–712, http://dx.doi.org/10.1016/j.engfailanal.2017.06.001, URL https://www.sciencedirect.com/science/article/pii/S1350630716308160.

[10] J. Zhang, H. Dai, J. Lin, Y. Yuan, Z. Liu, Y. Sun, K. Ding, Cracking analysis of an aero-engine combustor, Eng. Fail. Anal. (ISSN: 1350-6307) 115 (2020) 104640, http://dx.doi.org/10.1016/j.engfailanal.2020.104640, URL https://www.sciencedirect.com/science/article/pii/S1350630718310331.

[11] N. Ejaz, I. Qureshi, S. Rizvi, Creep failure of low pressure turbine blade of an aircraft engine, Eng. Fail. Anal. (ISSN: 1350-6307) 18 (6) (2011) 1407–1414, http://dx.doi.org/10.1016/j.engfailanal.2011.03.010, URL https://www.sciencedirect.com/science/article/pii/S135063071100063X.

[12] H. Zhang, C. Li, Q. Guo, Z. Ma, H. Li, Y. Liu, Improving creep resistance of nickel-based superalloy inconel 718 by tailoring gamma double prime variants, Scr. Mater. (ISSN: 1359-6462) 164 (2019) 66–70, http://dx.doi.org/10.1016/j.scriptamat.2019.01.041, URL https://www.sciencedirect.com/science/article/pii/S1359646219300582.

[13] J. Reeves, R. Remenyte-Prescott, J. Andrews, P. Thorley, A sensor selection method using a performance metric for phased missions of aircraft fuel systems, Reliab. Eng. Syst. Saf. (ISSN: 0951-8320) 180 (2018) 416–424, http://dx.doi.org/10.1016/j.ress.2018.07.029, URL https://www.sciencedirect.com/science/article/pii/S0951832017314631.

[14] A. White, A. Karimoddini, Event-based diagnosis of flight maneuvers of a fixed-wing aircraft, Reliab. Eng. Syst. Saf. (ISSN: 0951-8320) 193 (2020) 106609, http://dx.doi.org/10.1016/j.ress.2019.106609, URL https://www.sciencedirect.com/science/article/pii/S0951832018314030.

[15] J. Lee, M. Mitici, An integrated assessment of safety and efficiency of aircraft maintenance strategies using agent-based modelling and stochastic Petri nets, Reliab. Eng. Syst. Saf. (ISSN: 0951-8320) 202 (2020) 107052, http://dx.doi.org/10.1016/j.ress.2020.107052, URL https://www.sciencedirect.com/science/article/pii/S0951832020305536.

[16] J. Liu, F. Lei, C. Pan, D. Hu, H. Zuo, Prediction of remaining useful life of multi-stage aero-engine based on clustering and LSTM fusion, Reliab. Eng. Syst. Saf. (ISSN: 0951-8320) 214 (2021) 107807, http://dx.doi.org/10.1016/j.ress.2021.107807, URL https://www.sciencedirect.com/science/article/pii/S0951832021003306.

[17] P. Wen, S. Zhao, S. Chen, Y. Li, A generalized remaining useful life prediction method for complex systems based on composite health indicator, Reliab. Eng. Syst. Saf. (ISSN: 0951-8320) 205 (2021) 107241, http://dx.doi.org/10.1016/j.ress.2020.107241, URL https://www.sciencedirect.com/science/article/pii/S0951832020307419.

[18] Z. Li, D. Wu, C. Hu, J. Terpenny, An ensemble learning-based prognostic approach with degradation-dependent weights for remaining useful life prediction, Reliab. Eng. Syst. Saf. (ISSN: 0951-8320) 184 (2019) 110–122, http://dx.doi.org/10.1016/j.ress.2017.12.016, Impact of Prognostics and Health Management in Systems Reliability and Maintenance Planning, URL https://www.sciencedirect.com/science/article/pii/S0951832017308104.

[19] S. Zhong, Z. Tan, L. Lin, Long-term prediction of system degradation with similarity analysis of multivariate patterns, Reliab. Eng. Syst. Saf. (ISSN: 0951-8320) 184 (2019) 101–109, http://dx.doi.org/10.1016/j.ress.2017.11.001, Impact of Prognostics and Health Management in Systems Reliability and Maintenance Planning, URL https://www.sciencedirect.com/science/article/pii/S0951832017306221.

[20] H. Zhou, A.K. Parlikad, A. Brintrup, Data-driven maintenance priority recommendations for civil aircraft engine fleets using reliability-based bivariate cluster analysis, Qual. Eng. (2023) 1–16, http://dx.doi.org/10.1080/08982112.2022.2163179.

[21] H. Zhou, M. Farsi, A. Harrison, A.K. Parlikad, A. Brintrup, Civil aircraft engine operation life resilient monitoring via usage trajectory mapping on the reliability contour, Reliab. Eng. Syst. Saf. (ISSN: 0951-8320) 230 (2023) 108878, http://dx.doi.org/10.1016/j.ress.2022.108878, URL https://www.sciencedirect.com/science/article/pii/S0951832022004951.

[22] Z. Wang, Z. Wang, S. Yu, K. Zhang, Time-dependent mechanism reliability analysis based on envelope function and vine-copula function, Mech. Mach. Theory (ISSN: 0094-114X) 134 (2019) 667–684, http://dx.doi.org/10.1016/j.mechmachtheory.2019.01.008, URL https://www.sciencedirect.com/science/article/pii/S0094114X18311455.

[23] E. Okafor, E. Ezugwu, P. Jemitola, Y.-C. Sun, Z. Lu, Multistate system reliability modeling using copula function, in: 2018 3rd International Conference on System Reliability and Safety, ICSRS, 2018, pp. 135–141, http://dx.doi.org/10.1109/ICSRS.2018.8688860.

[24] Z. Yongjin, S. Youchao, L. Longbiao, Z. Ming, Copula-based reliability analysis for a parallel system with a cold standby, Comm. Statist. Theory Methods 47 (3) (2018) 562–582, http://dx.doi.org/10.1080/03610926.2017.1309432.

[25] X.-S. Tang, D.-Q. Li, C.-B. Zhou, K.-K. Phoon, Copula-based approaches for evaluating slope reliability under incomplete probability information, Struct. Saf. (ISSN: 0167-4730) 52 (2015) 90–99, http://dx.doi.org/10.1016/j.strusafe.2014.09.007, URL https://www.sciencedirect.com/science/article/pii/S0167473014000903.

[26] X.-S. Tang, D.-Q. Li, C.-B. Zhou, L.-M. Zhang, Bivariate distribution models using copulas for reliability analysis, Proc. Instit Mech Eng Part O: J. Risk Reliabil. 227 (5) (2013) 499–512, http://dx.doi.org/10.1177/1748006X13481928.

[27] E.L. Kaplan, P. Meier, Nonparametric estimation from incomplete observations, J. Amer. Statist. Assoc. (ISSN: 01621459) 53 (282) (1958) 457–481, http://dx.doi.org/10.2307/2281868, URL http://www.jstor.org/stable/2281868.

[28] F. Durante, J. Fernández-Sánchez, C. Sempi, A topological proof of Sklar's theorem, Appl. Math. Lett. (ISSN: 0893-9659) 26 (9) (2013) 945–948, http://dx.doi.org/10.1016/j.aml.2013.04.005, URL http://www.sciencedirect.com/science/article/pii/S0893965913001183.

[29] C. Genest, L.-P. Rivest, Statistical inference procedures for bivariate archimedean copulas, J. Amer. Statist. Assoc. 88 (423) (1993) 1034–1043, http://dx.doi.org/10.1080/01621459.1993.10476372, URL https://www.tandfonline.com/doi/abs/10.1080/01621459.1993.10476372.

[30] E. Kole, K. Koedijk, M. Verbeek, Selecting copulas for risk management, J. Bank. Financ. (ISSN: 0378-4266) 31 (8) (2007) 2405–2423, http://dx.doi.org/10.1016/j.jbankfin.2006.09.010, URL http://www.sciencedirect.com/science/article/pii/S0378426607000362.

[31] S. Demarta, A.J. McNeil, The t copula and related copulas, Internat. Statist. Rev. 73 (1) (2005) 111–129, http://dx.doi.org/10.1111/j.1751-5823.2005.tb00254.x, URL https://onlinelibrary.wiley.com/doi/abs/10.1111/j.1751-5823.2005.tb00254.x.

[32] H. Joe, Asymptotic efficiency of the two-stage estimation method for copula-based models, J. Multivariate Anal. (ISSN: 0047-259X) 94 (2) (2005) 401–419, http://dx.doi.org/10.1016/j.jmva.2004.06.003, URL https://www.sciencedirect.com/science/article/pii/S0047259X04001289.

[33] B. De Baets, H. De Meyer, On a conjecture about the Frank copula family, Fuzzy Sets and Systems (ISSN: 0165-0114) 228 (2013) 15–28, http://dx.doi.org/10.1016/j.fss.2012.07.007, Special issue on AGOP 2011 and EUSFLAT/LFA 2011, URL https://www.sciencedirect.com/science/article/pii/S0165011412003077.

[34] J. Hauke, T. Kossowski, Comparison of values of pearson's and spearman's correlation coefficients on the same sets of data, Quaestiones Geogr. 30 (2) (2011) 87–93, http://dx.doi.org/10.2478/v10117-011-0021-1, URL https://content.sciendo.com/view/journals/quageo/30/2/article-p87.xml.

[35] M.G. Kendall, A new measure of rank correlation, Biometrika (ISSN: 0006-3444) 30 (1–2) (1938) 81–93, http://dx.doi.org/10.1093/biomet/30.1-2.81, arXiv:https://academic.oup.com/biomet/article-pdf/30/1-2/81/423380/30-1-2-81.pdf.

[36] H. Zhou, S. Gnanasambandam, M. Foresta, F. Li, M.L. Blanc, D. Weston, J. Pan, Life prediction of phosphor bronze reinforcing tape used in underground power cables, Corrosion (ISSN: 0010-9312) 74 (5) (2017) 530–542, http://dx.doi.org/10.5006/2627.

[37] H. Zhou, S. Gnanasambandam, M. Foresta, D. Weston, F. Li, J. Pan, M. Le Blanc, Measurement and modeling of pitting depth distribution for phosphor bronze tapes used in underground power transmission cables, Corrosion (ISSN: 0010-9312) 73 (7) (2017) 844–852, http://dx.doi.org/10.5006/2227.

[38] J.Y. Hesterman, L. Caucci, M.A. Kupinski, H.H. Barrett, L.R. Furenlid, Maximum-likelihood estimation with a contracting-grid search algorithm, IEEE Trans. Nucl. Sci. 57 (3) (2010) 1077–1084, http://dx.doi.org/10.1109/TNS.2010.2045898.